Hindawi
Wireless Communications and Mobile Computing
Volume 2022, Article ID 4658082, 12 pages
https://doi.org/10.1155/2022/4658082

Research Article

A Compact Frequency and Radiation Reconfigurable Antenna for 5G and Multistandard Sub-6 GHz Wireless Applications

Shakir Ullah,[1] **Issa Elfergani**,[2,3] **Inzamam Ahmad**,[1] **Iftikhar Ud Din**,[1] **Sadiq Ullah**,[1] **Wasi Ur Rehman Khan**,[1] **Toufeeq Ahmad**,[1] **Usman Habib**,[4] **Chemseddine Zebiri**,[5] **and Jonathan Rodriguez**[2]

[1]*Department of Telecommunication Engineering, University of Engineering & Technology, 23200 Mardan, Pakistan*
[2]*Instituto de Telecomunicações, Campus Universitário de Santiago, Aveiro 3810-193, Portugal*
[3]*School of Engineering and Informatics Bradford University, Bradford BD7 1DP, UK*
[4]*Faculty of Engineering Sciences, GIK Institute of Engineering Sciences and Technology, Topi 23640, Pakistan*
[5]*Laboratoired'Electronique de Puissance et Commande Industrielle (LEPCI), Dept. of Electronics, University of Ferhat Abbas, Sétif -1-, 19000 Sétif, Algeria*

Correspondence should be addressed to Shakir Ullah; shakirhayat.eng@gmail.com

Received 20 October 2021; Revised 18 January 2022; Accepted 25 January 2022; Published 10 February 2022

Academic Editor: Enrico M. Vitucci

This paper presents a reconfigurable antenna operating in three modes at different frequency bands with pattern reconfiguration. Frequency and pattern reconfigurability are achieved using four PIN diodes. In particular, two diodes are mounted in the radiating part of the hexagon shape to perform the frequency reconfiguration of the antenna. The other two PIN diodes are connected with the inverted L-shaped and CPW ground by changing the main lobe beam steering to achieve the pattern reconfiguration. An antenna has been designed, fabricated, and numerically and experimentally assessed. The prototype of the antenna is fabricated on a commercially available FR-4 substrate of thickness 1.6 mm ($\varepsilon_r = 4.3$). Thus, the proposed antenna supports several 5G sub-6 GHz bands (3.1 GHz, 4.1 GHz, and 3.8 GHz), WiFi (2.45 GHz), as well as (7.8 GHz, 9.5 GHz) X-Band Satellite applications. The obtained results are quite promising. In particular, it is observed that the measured results are in close agreement with the simulation results, and the proposed (compact) antenna prototype can be a prospective candidate for future portable devices, sensor networks, and telecommunication applications.

1. Introduction

Reconfigurable antennas are a promising solution to provide operation in several frequency bands or patterns, depending on the design and network requirements [1], and are becoming a research focus for several wireless transmission standards. For antennas with the capability to serve users at different frequencies and different communication standards, the desired band is tuned by redistribution of the antenna properties, which then resonates accordingly. Considering the high congestion of the available frequency spectrum, the use of reconfigurable antennas is mandatory to provide efficient use of the available frequency bands [2]. The other type provides reconfiguration of the radiation pattern, which is achieved by rearranging the radiating current or edges of the antenna [3]. A major application for such designs is beam steering, where the focused beam is directed towards the intended use for gain enhancement, improved energy efficiency, and reduced interference from other in-band radiations [4, 5]. Such factors not only improve the overall transmission data rate through an increase in channel capacity but are crucial for frequency selective channel transmission. The use of configurable antennas is certainly quite interesting, but the requirements to provide adequate gain and stable operation in each transmission band or direction become a challenge for antenna design engineers. For the RF antennas, reconfiguration can be achieved by altering the electrical, mechanical, or material

characteristics. Phased array and fully adaptive array offer very good beam pattern customization capabilities, but they are quite expensive, bulky, and not suitable for handy devices. Most of the existing designs are based on the characterization of a single parameter to cope with the complexity involved. For example, a differential antenna design for reconfiguring frequency characteristics is presented in [6], and such designs can be extended to operate in several frequency bands, such as WLAN standards of WiFi, UTMS, and WiMAX [7]. To make such an antenna compatible with wearable or airborne applications, a low-profile design in [8] provides operation in the ISM and airport radar bands. As 5 G and future mobile access networks are standardizing several bands in the sub-6 GHz spectrum range, reconfigurable antennas with differentially fed [9] have shown the potential of reconfiguration for various mobile applications.

The other set of configurable antennas, which provide various patterns, has also been reported in recent literature. In [10], a Yagi-Uda antenna design is shown with the switching function to operate in either an omnidirectional or bidirectional mode. A partially reflective surface (PRS) based pattern reconfigurable design is presented in [11], which provides beam steering for the angles of +78°, 0°, and -78° with a high gain at the operating frequency of 1.8 GHz. A similar design for wireless sensor network (WSN) is reported in [12] for a license-free ISM band of 2.4 GHz to steer the beam in four different directions (0°, 90°, 180°, and 270°). The optimization of the state transition for such antennas can be performed using genetic algorithms [13] to achieve a smooth transition among different defined states. A variety of pattern tunable antennas are reported based on different configurations, such as complementary split-ring resonators (CSRR) on the ground [14] and a very popular method of using micro-electro-mechanical switches (MEMS) with coupling cells. Due to the increased interest in slot antennas for future wireless applications [15], they have also been presented in a frequency and pattern reconfigurable design [16]. In the CPW feed-based reconfigurable antenna design [17], the reconfiguration is achieved through two pin-diodes for achieving frequency reconfigurability for the 1.65–2.51 GHz band while pattern reconfigurability along +90° and -90° for the respective band. Similar frequency and pattern reconfiguration have also been shown to be achieved using two Varactor diodes in [18], with a wider beam direction range of -23° to +23°. Reference [19] presents frequency and pattern reconfigurable antennas, using fourteen switches and electromagnetic bandgap (EBG) unit cells. The antenna is optimally suited for 2.4 and 5.8 GHz WLAN operation. Other useful designs include the use of electromagnetic bandgap (EGB) unit cells containing pin diodes for frequency selectivity [20].

For [17–21], the size of the antenna is the major drawback to being used for compact and wearable applications. The presented designs in [22–24] are compact but can offer a smaller number of bands and beam steering by using more switches and bandwidth up to 500 MHz. The most considerate design in [25] with its small size and large bandwidth also imposes a challenge to use 8 switches and a provision of 3.8 dB gain as a maximum.

This work proposes a novel design to obtain a very compact antenna, by using only four PIN diode switches, and it provides a gain of up to 4.25 dB with large bandwidth operation. The presented antenna provides adequate gain and bandwidth with good reconfigurable capabilities, and it results in more compact in size with respect to the state-of-the-art antennas present in scientific literature. The four pin-diode switches provide the rearrangement of the compound, with two switches (D1 and D2) responsible for the shifting of frequency bands and two (D3 and D4) for steering the directional beam. Moreover, the design allows the antenna to operate in three different modes to select a particular frequency band and its related pattern. In terms of bands, the design offers dual-band operation at 3.1 and 7.8 GHz in mode 1. 3.1 GHz has been previously considered for ground surveillance radars and radiolocation [26], but has now been actively used for Earth exploration (EE) services and space research [27]. The X-band (8 to 12 GHz) is considered for handheld satellite receivers and is included in the presented design. For band selectivity, the frequency bands of 2.4, 4.1, 9.5 GHz, and 3.8 GHz are selected using mode 2 and mode 3, respectively. The simulation results demonstrate the effectiveness of beam steering operation at nine angular locations for frequency sets of 2.4, 4.1, and 9.5 GHz and three angular directions for 3.8 GHz bands. To ensure the compatibility of the design with 5G standards for sub-6 GHz transmission, the detailed analysis shows the antenna operation at 2.4, 3.1, 4.1, and 3.8 GHz. The different states of pin-diodes allow either a single band, dual-band, or tri-band operation. The main contributions of the presented work are as follows:

(i) The designed antenna is compact as compared to the previously published work in this research area, with the added benefits of multiband mode, increased bandwidth, and gain.

(ii) To the best of the authors' knowledge, the design offers the highest number of beam directions with a frequency selectivity of five bands, which is the first of its kind as compared to the state-of-the-art.

(iii) Being highly compatible with 5G services due to large bandwidth, sub-6 GHz operation and moderate gain is also a distinct feature of an antenna with both frequency and pattern reconfigurability.

The rest of the paper is organized in the following way. The design methodology and antenna geometry are described in Section 2. Different stages involved in the evolution of the final design are presented in Section 3. The experimental results and analysis are discussed in Section 4 along with a brief comparison with the most recently published works. Finally, Section 5, reports the conclusions.

2. Design Methodology and Antenna Geometry

Figure 1 shows the antenna geometry and the related geometrical parameters. The antenna structure reported in Figure 1 consists of a main hexagonal radiator connected with two parasitic structures. The antenna is fed with a coplanar waveguide (CPW), characterized with an

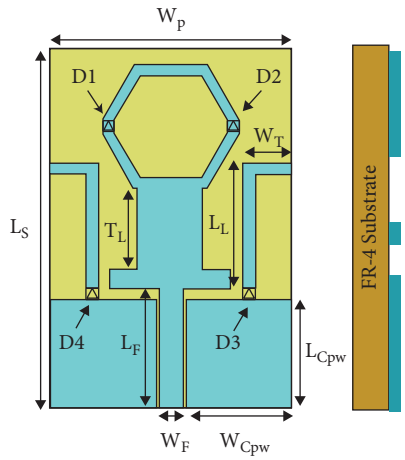

Figure 1: Schema of the proposed antenna, front and side views.

impedance of 50 Ohms, the CPW width id $W_f = 3$ mm, estimated with the well-known semi-analytical Hammerstad formula and considering a commercial FR-4 dielectric substrate with a thickness of 1.6 mm, relative permittivity, ε_r of 4.3, and loss tangent, δ of 0.025. Initially, the antenna geometry is composed of a size of $30 \times 20 \times 1.6\,\text{mm}^3$. The details of each parametric dimension of the design are given in Table 1, and they have been obtained after a detailed parametric analysis.

To achieve a particular frequency operation, the following relation aimed at estimating the L_f parameter has to be considered [2]:

$$L_f = \frac{c}{4f\sqrt{\mathscr{E}_{\text{eff}}}}, \tag{1}$$

where

$$\mathscr{E}_{eff} = \frac{\mathscr{E}_r + 1}{2} + \frac{\mathscr{E}_r - 1}{2}\left(1 + 12\left(\frac{w}{h}\right)\right)^{-0.5}, \tag{2}$$

here "c" represents the velocity of the light in a vacuum, "h" is the thickness, and "w" is the substrate's width. In such designs, two parasitic patches are utilized in the radiating structure. The parasitic patches are connected to the main radiator with pin diodes (SMP1345-079LF) switches. The status of the connection between the patches (open or short), controlled by the two pin diodes (ON or OFF), defines the effective resonant length, and hence the operating conditions of the antenna in terms of frequency. Two additional pin diodes switches are integrated at the rear side of the antenna as switches for pattern reconfiguration. These pattern-related control switches are installed in the L-shaped stubs to redistribute the concentration of the surface currents. This causes the antenna to operate with a different pattern with adequate gain and impedance matching, as the L-shaped inverted stubs were introduced in the CPW ground plane. The front geometric view of these stubs is shown in Figure 1.

2.1. Switching Technique. For any frequency band, the pin diodes (SMP1345-079LF) work as an electronic switch. But the working principle is different as the control element is the resonant length, which is varied to achieve frequency and pattern reconfigurability. Figure 2 shows the equivalent circuits when pin diodes are used in ON and OFF states. A simple RL series circuit is formed for the ON state with extremely low resistor "R_L" and an inductor "L." For the OFF state, the circuit becomes RLC with a parallel inductor "L," along with a resistor of a high value "R_H", and a capacitor "C". For fabrication, the model of PIN diode Skyworks SMP1345-079LF is chosen for its low cost and ease of availability. The parametric values from the datasheet can easily be modeled in the CST simulation environment as $C = 0.15$ pF, $L = 0.7$ nH, and $R_L = 1.5\,\Omega$. Table 2 explains the switching arrangements for all the cases of three operating modes.

Table 1: Proposed antenna geometrical design parameters.

Parameters	Size (mm)
L_T	1
W_T	10
L_P	7
W_P	5.5
H_s	1.6
L_f	10
L_T	1
W_f	3
L_{s1}	30
W_{s1}	20
W_{cpw}	8.5
L_{cpw}	9
W_f	3
L_{s1}	30

The biasing circuit has been introduced on the backside of the antenna during measurement setup for operating the pin diode in Real-time, as shown in Figure 3. Figure 3 also shows the control circuit of the PIN diode switches, and the measurement setup for only mode 2 when one of the switches of the hexagon (the main radiator) is operated for frequency reconfiguration in a real-time environment and the rest of all the modes were operated one by one during testing of the antenna.

3. Development for the Design Optimization

The different design steps are shown in Figure 4, and the related results in terms of return loss characteristics are reported in Figure 5. The synthetic results of Figure 5 have been obtained with a commercial electromagnetic simulator, namely CST Microwave Studio. A tuning phase has been made for improvement in antenna performance in terms of driving point impedance bandwidth and return loss. Figure 4 depicts that step 2 is designed by introducing a rectangular patch upon a T-shape in step 2 with a wide band of the operating frequency of 4.53 GHz–9.50 GHz. The hexagonal shape is embedded on the top in step 3 with dual-band operation of 3.09 GHz (2.74 GHz–3.48 GHz) and 8.17 GHz (7.26 GHz–8.82 GHz) along with the introduction of L-stubs to the left and right in sep4 and step5 simultaneously with the resonance of 2.32 GHz (2.20 GHz–2.41 GHz) and 8.5 GHz (7.22 GHz–9.20 GHz) finally

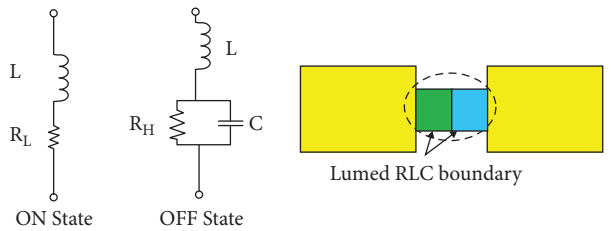

Figure 2: Equivalent circuit of PIN diode model [28].

Table 2: Different modes of switching.

Mode	Special cases
Mode-1 (S1 = ON, S2 = ON)	C1 (S1 to S4 = ALL ON), C2 (S1, S2, S3 = ON, S4 = OFF), C3 (S1, S2, S4, ON, S3 = OFF)
Mode-2 (S1 = ON, S2 = OFF)	C1 (S2, S3, S4 = OFF, S1- = ON), C2 (S2, S3 = OFF, S1, S4 = ON), C3 (S1, S3 = ON, S2 = S4 = OFF)
Mode-3 (S1 = OFF, S2 = OFF)	C1 (S1 to S4 = all OFF), C2 (S1, S2, S4 = OFF, S3 = ON), C3 (S1, S2, S3 = OFF, S4 = ON)

(C represents the case here).

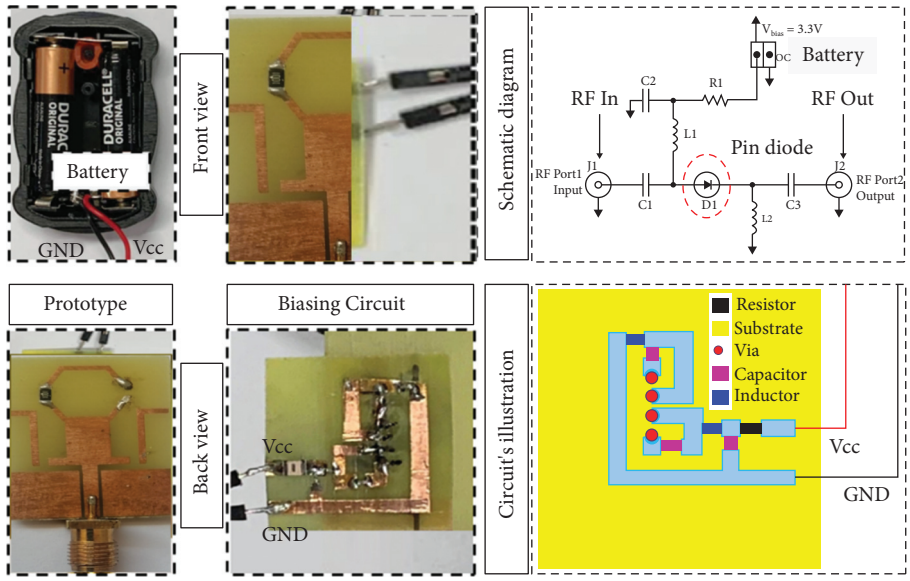

Figure 3: Equivalent circuit of PIN diode model.

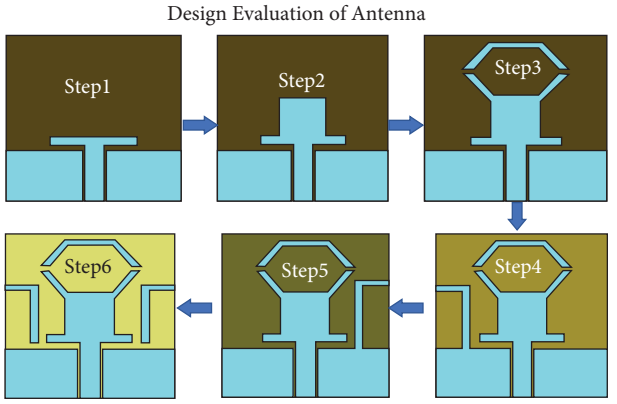

Figure 4: Various design steps for the evaluation of the proposed antenna.

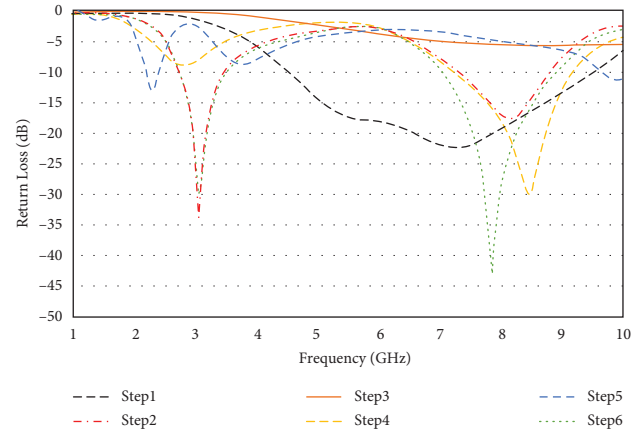

Figure 5: The return loss of the design evaluation.

to achieve the proposed antenna design with two L-shape stubs on the left and right side of the hexagonal shape. It is evident from Figure 5 that the stepwise modifications improve the return loss of the proposed design. For various switching states, the antenna S-parameters are observed by inserting a stub with the CPW plan.

Figure 6 shows that for case 1, when an F-shaped stub is connected to the ground, 3.1 GHz and 7.3 GHz are selected by the antenna as resonant frequencies. For case 2, the antenna provides a good impedance match at 2.24 GHz, 4.12 GHz, and 9.12 GHz. A single band operation is obtained for case 3 at 4.01 GHz. Figure 7 shows the following step where the CPW plane is loaded with the L-shaped stub. The two switches of the stub are aimed at refining the frequency selectivity from the previous step. As it can be seen, when only switch 1 is turned ON, the antenna resonates at 3.5 GHz and 7.3 GHz. The resonant frequency becomes 2.10 GHz, 4.23 GHz dual-band, and 3.91 GHz for the previously mentioned case 1 and case 2. A reasonable impedance match is seen in case 3 for 3.01 GHz and 7.12 GHz. Finally, an L-shaped stub is introduced in the CPW plane, and its impact during all four cases can be noted from Figure 8. This shows that for all four cases, the antenna provides good performance in terms of the reflection coefficient.

4. Experimental Analysis and Results

To verify the design and simulation outcomes, the antenna is fabricated, and experimental work is performed at an anechoic chamber in the National University of Science and Technology (NUST). The fabricated antenna is equipped with a coaxial subminiature type A (SMA) connector, as shown in Figure 9, along with the measurement setup consisting of a turntable and RF cables in the chamber. The whole measurement setup is first calibrated, and several sets of measurements are performed to validate the performance of the fabricated antenna. The scattering parameter has been measured with a vectorial network analysis.

The proposed design is capable of working in three different modes and cases, each providing a particular frequency band operation with different reconfiguration patterns. The return loss experimental results are shown in Figure 10 for the antenna operating in mode 1. The numerical results, obtained with the CST software, are also plotted to show the agreement with the measured ones. Figures 11 and 12 show the results for an antenna operating in mode 2 and mode 3, respectively. It is evident from return loss plots that the proposed design provides good impedance matching for all operating scenarios.

These results show a good deal of validation for experimental results. Figure 13 shows the measured antenna gain versus operating frequency for all switching modes. Finally, for the three switching modes, the radiation pattern plots are outlined in Figures 14–16, while the surface current distributions are depicted in Figures 17–19. The detailed discussion of the obtained results for the three modes (1, 2, and 3) is as follows.

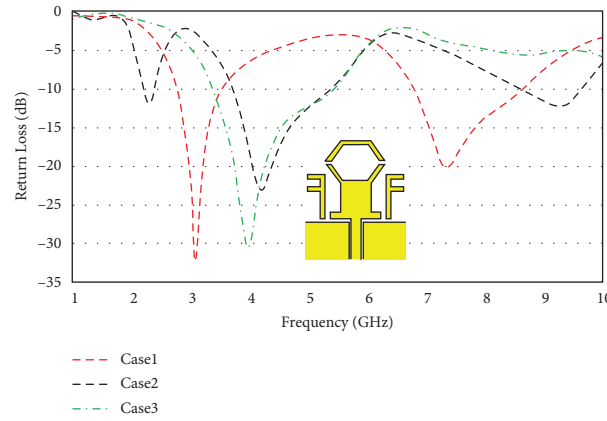

Figure 6: Reflection coefficient analysis for F-shaped stub.

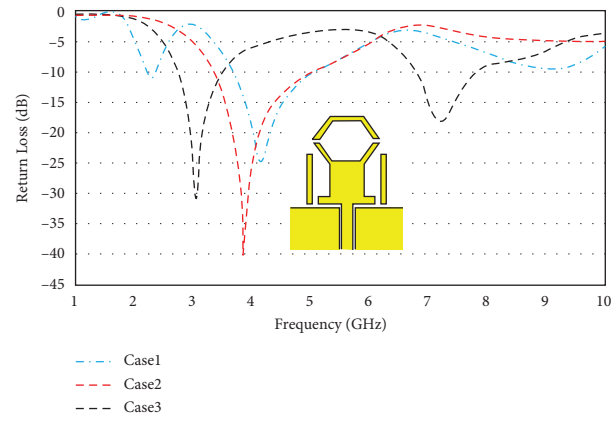

Figure 7: Reflection coefficient analysis for I-shaped stub.

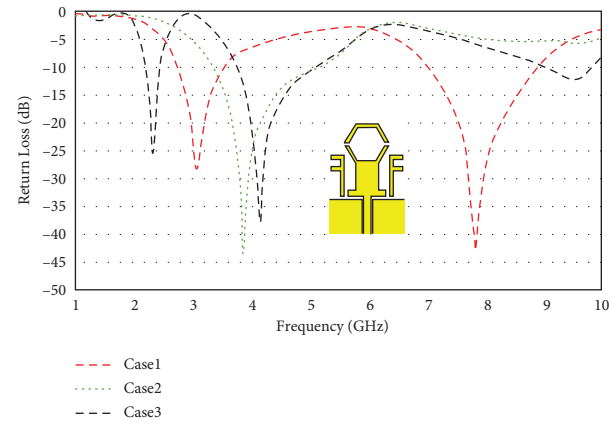

Figure 8: Reflection coefficient analysis for L-shaped stub.

4.1. Results for Mode 1 Operation. Case 1 (of mode 1) is activated by turning ON all the switches and the dual-band operation is actuated covering 3.1 GHz and (2.74–3.52 GHz) and 7.8 GHz band (7.01–8.93 GHz). As shown in Figure 13, the two center frequencies of 3.1 and 7.8 GHz are selected in this case, and the H-plane main beam is directed (Phi = 0) at 180°, -30°, and 30°. The second case of mode 1 is activated by turning OFF the switch S4, which makes the radiation pattern steered along -120° and -30°. When the switch S3 is

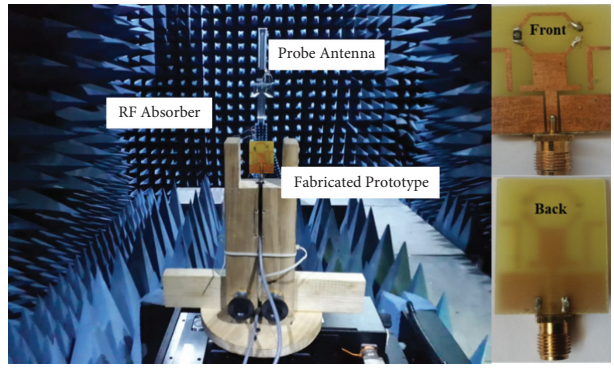

Figure 9: Anechoic chamber and fabricated prototype.

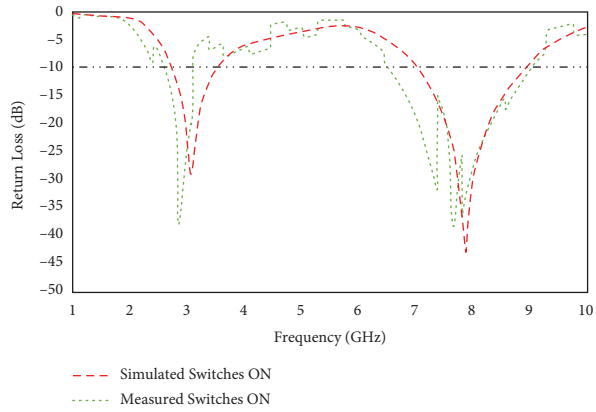

Figure 10: Mode 1 simulated and measured return loss.

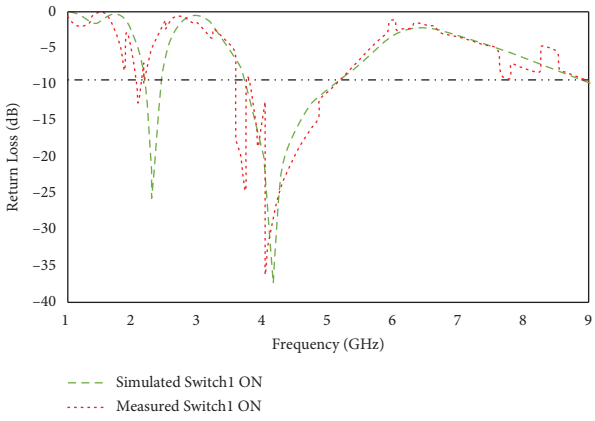

Figure 11: Mode 2 simulated and measured return loss.

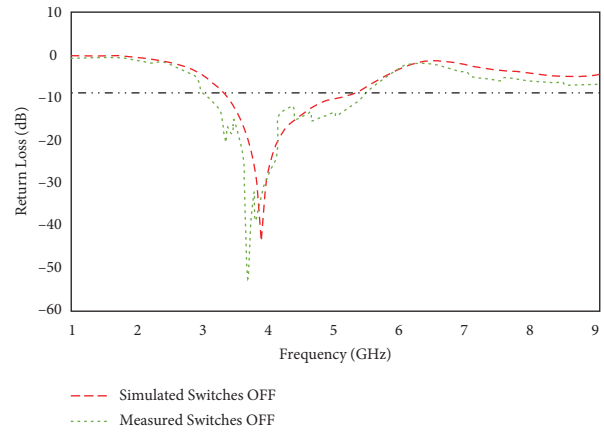

Figure 12: Mode 3 simulated and measured return loss.

turned OFF, the third case of mode 1 is activated, and the beam is steered towards +120° and +30°, as can be noticed from the experimental results in Figure 14.

4.2. Results for Mode 2 Operation. Figure 15 shows the results for mode 2, obtained by turning ON the switch S2. This makes the antenna resonate at the frequencies of 2.45 GHz, 4.1 GHz, and 9.5 GHz. For case 1 of mode 2, the 10 dB bandwidth can be evaluated from the frequency range 3.09 GHz–4.17 GHz as shown by the measured results. The directional pattern shows that the beam is directed towards 180°, 180°, and 115°. Case 2 of this mode is picked when switches S2 and S4 are in ON conditions, while the third case is activated when S2 and S3 are in ON states. The frequency selectivity for both cases covers the tri-band values of 2.45 GHz, 4.1 GHz, and 9.5 GHz. The beam pattern plots are reported in Figure 15, which shows the beam steering characteristics for the three cases where, for 2.45 GHz, 4.1 GHz, and 9.5 GHz, the main beam is directed along +150°, +90° and (-30° and -50°) in the second case and along -150°, -90°, and (-120° and 150°) in the third case.

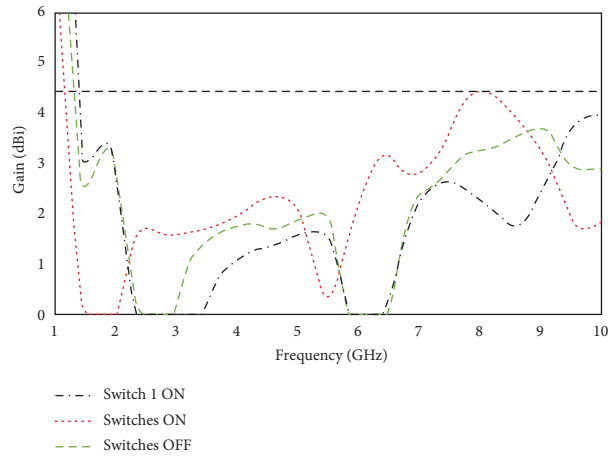

Figure 13: Gain vs frequency graph for three operating modes.

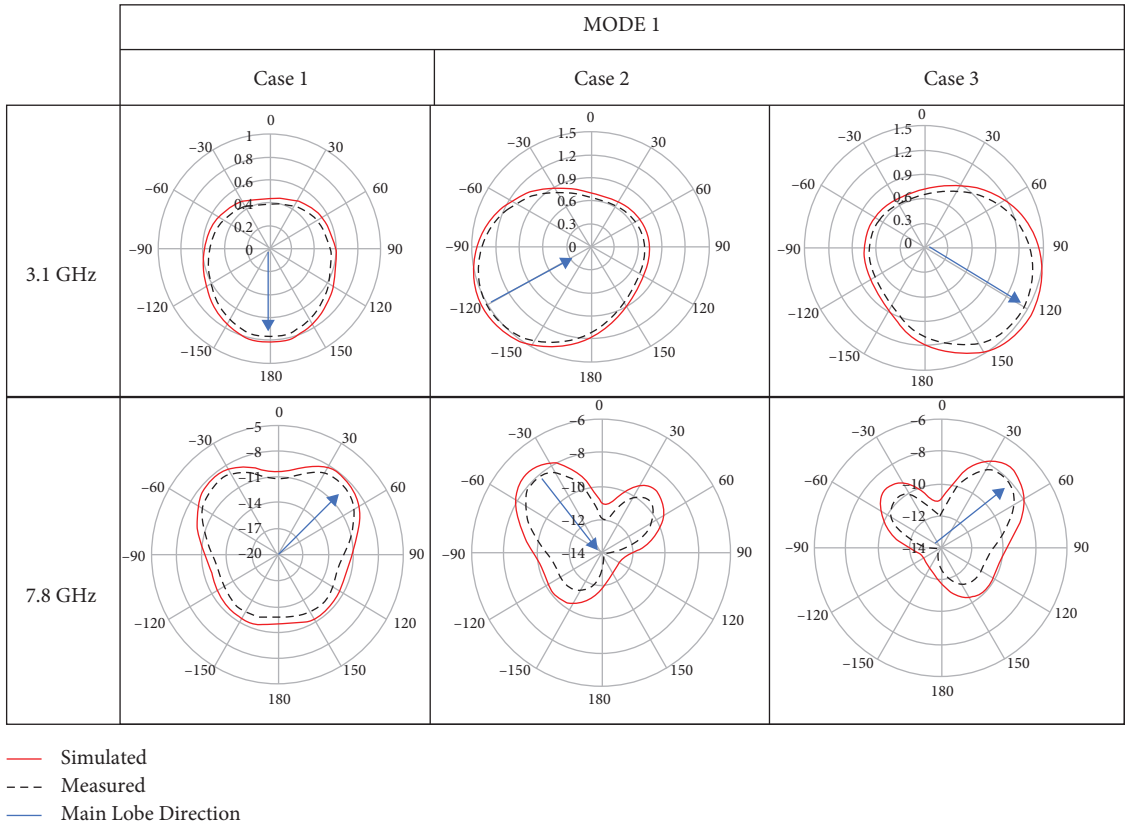

Figure 14: Polar plots (at phi = 0, x-z plane) for case1–3 of mode1 for 3.1 and 7.8 GHz.

4.3. Results for Mode 3 Operation. Case 1 of mode 3 operation is attained by switching OFF S1 and S2. This is a single-band operation with large bandwidth covering a 3.36 GHz–5.17 GHz range and points the directional beam towards 180°.

The operation in mode 3 is shifted to case 2 by keeping the S1, S3 OFF and turning ON the switches S2, S4, which shifts the beam to -90°. Finally, the 3rd case is picked when switches S1 to S3 are ON and S4 is OFF which steers the beam along 90°. The main beam direction with the peak gain, for all the considered operative cases, is outlined in Table 3, as well as the shifting of the beam angle. For each operating frequency, this is the degree to which the antenna beam is shifted.

The summary of the antenna performance in terms of different frequency selectivity, gain, and beam steering is given in Table 4. Figures 17–19 provide the detailed insight of surface currents for modes 1–3, where the resonant areas can be seen to contribute towards a specific operating state. For example, the surface current of case 1 for all modes represents the frequency reconfigurable characteristics and consists of information about resonant length. It can be

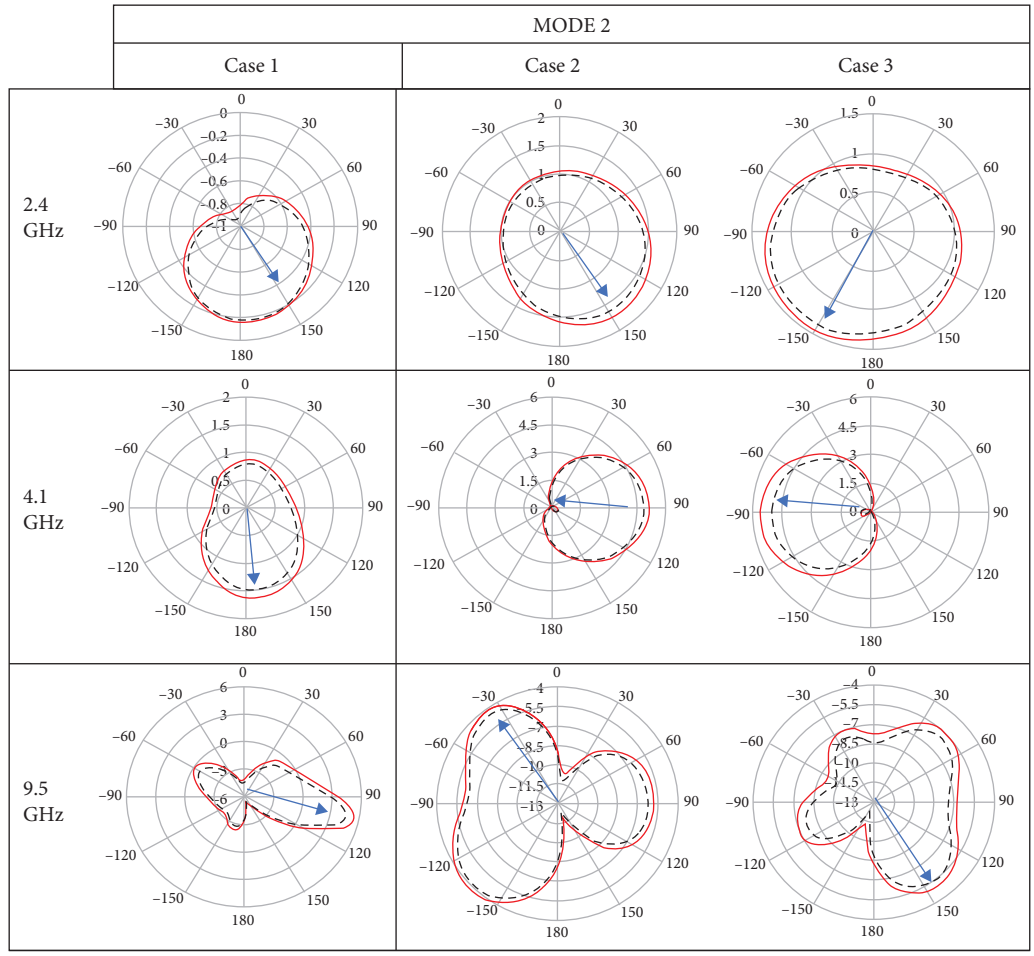

Figure 15: Polar plots (at phi = 0, x-z plane) for case1–3 of mode2 for 2.4, 4.1, and 9.5 GHz.

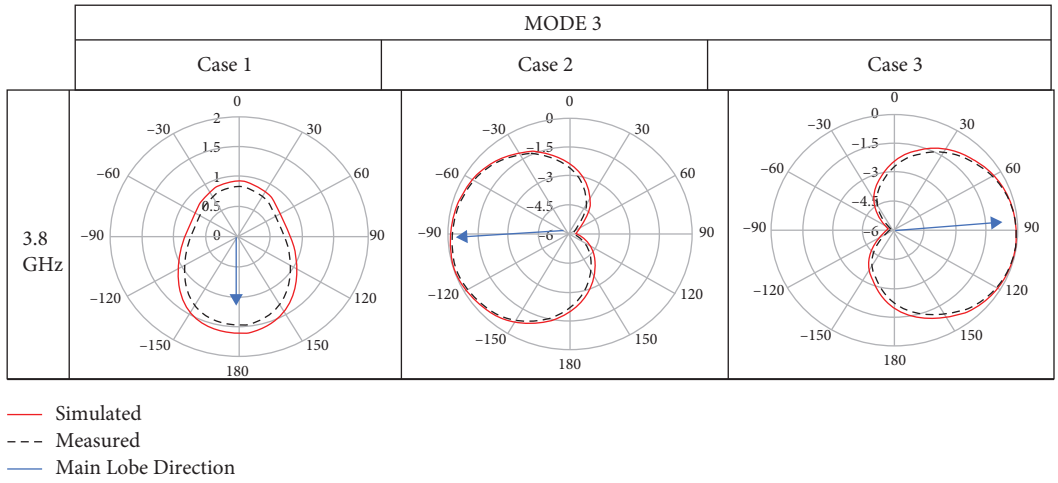

Figure 16: Polar plots (at phi = 0, x-z plane) mode3 for all cases.

observed that a reduction in effective resonant length leads to an increase in resonant frequency, thus validating the inverse relationship. Cases 2 and 3 demonstrate the pattern reconfigurability with information about the effective stub length to achieve beam steering in a particular direction. The active portion is illustrated for the stubs to understand the

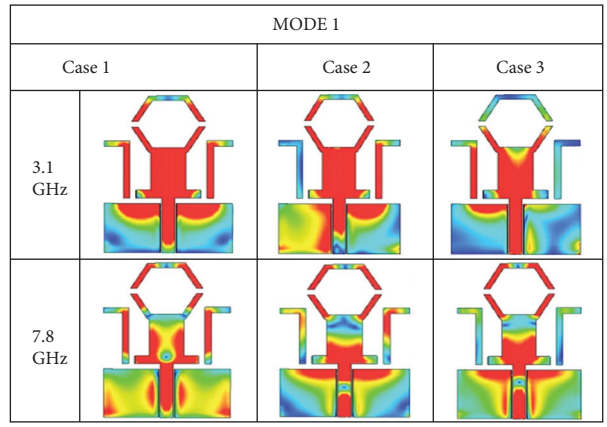

Figure 17: Surface currents for case 1, case 2, and case 3 of mode 1.

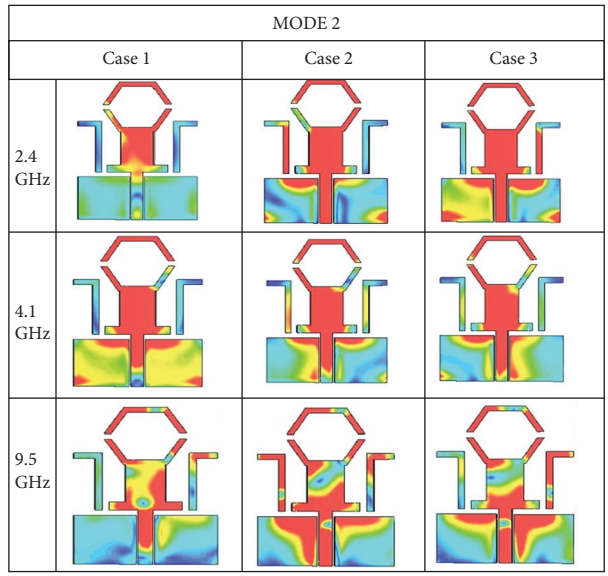

Figure 18: Surface currents for case 1, case 2, and case 3 of mode 2.

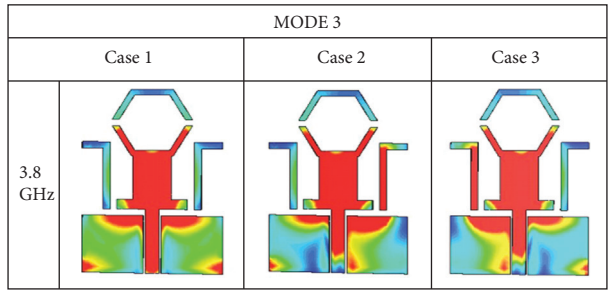

Figure 19: Surface currents of mode 3 for all cases.

directivity reconfiguration. The previously provided polar plots can be related to the surface currents. When the stubs are not contributing to the pattern reconfigurability in case 1 of mode 1, the antenna radiates in the direction of 180° and (+40°, -40°). When switches S1–S3 are turned ON in case 2, the distribution of the surface currents changes and the right-side stub can be observed to play a significant role to shift the beam towards -120° and -40°. Lastly, for case 3, when switching S1, S2, and S4 are turned ON only with S3 being OFF, the left-side stub becomes dominant and results in the steering of the beam to +120° and +40°. In the same way, the other cases can be verified for polar plots and surface current results. Finally, Table 4 summarizes and compares different state-of-the-art antennas, demonstrating the effectiveness and capabilities of the proposed antenna, especially in terms of compactness.

Table 3: Performance parameters of the antenna.

Mode no	All cases	Operating frequency (GHz)	Bandwidth $f_l - f_u$ (MHz)	Gain (dB)	Direction of the beam at Phi = 0°	Angle of beam shifting
1	(1) all diodes are ON	3.1	2.74–3.52 (775)	1.56	180° -120°	0° -60°
	(2) D1–D3 are ON and D4 off (3) D1–D4 are ON and D3 OFF	7.8	7.01–8.93 (1874)	4.24	120° +40° 40° 50°	60° +140° -140° 130°
2	(1) D1, D2. D3 are OFF and D4 ON	2.45	2.19–2.44 (243)	1.67	+150° +150°	+30° +30°
	(2) D1, D3 are OFF and D2, D4 ON	4.1	3.76–5.12 (1358)	1.68	-150 +180 +90° -90°	-30° +0° +90° -90°
	(3) D2 = D3 = ON, D1 = D4 = OFF	9.5	9.12–9.84 (719)	3.49	+100° -30° +150°	+80° -150 +30°
3	(1) all diodes are OFF	3.8	3.36–5.17 (1808)	1.69	180°	0°
	(2) D1 = D2 = D4 = OFF, D3 = ON				-90	-90°
	(3) D2 = D3 = ON, D1 = D4 = OF				+90	+90°

Table 4: Comparison of different key performance indicators with state-of-the-art published work.

Reference	Antenna size (mm)	Number of switches	Number of operating bands	Number of beams	Bandwidth (MHz)	Peak gains (dBi)
[17]	45 × 50	2	1	3	800	2.2
[18]	160.9 × 151.5	2	2	2	730	9
[19]	113 × 113	14	2	3	NG	6.2/6.6
[20]	70 × 70	6	2	3	NG	5.08/7.0
[21]	112 × 52	18	2	8	1400/1501	3.8/8.3
[22]	50 × 50	4	1	3	1500/1200/1400	9.1/6.6/7.4
[23]	42 × 44	8	2	2	160/220	NG
[24]	40 × 30	4	2	3	400/500	2.24/2.76
[25]	31 × 27	8	6	7	410/1080/5500	`1.72/1.94/2.51/2.81/3.66/3.8
This work	30 × 20	4	5	9	410/1508/1880	`1.72/1.94/2.51/3.66/4.25

(NG: not given).

5. Conclusion

A novel design for a frequency and pattern reconfigurable antenna was designed, fabricated, and numerically and experimentally assessed for compact and multiband applications. The radiating antenna properties are set by using PIN diode switches. In particular, four PIN diodes are employed as switches for the compound reconfiguration where two of them (S1, S2) provide frequency selectivity and the remaining two (S3, S4) steer the beam in different angular directions. Three modes are presented for antenna operation in which different frequency bands demonstrate beam steering. The covered frequency bands consist of dual-band operation in 3.1 GHz and 7.8 GHz using mode1 (when all switches are ON of hexagon shape). The antenna operates at the triple band of 2.4, 4.1, and 9.5 GHz in mode 2 (when either S1 or S2 is ON) and a single band of 3.8 GHz band in mode 3 (when both S1, S2 are OFF). The obtained results demonstrate the ability of the antenna to provide beam steering in nine directions. The antenna can control the beam for five different operating bands of 3.1 GHz, 7.8 GHz (mode 1), 2.4 GHz, 4.1 GHz, 9.5 GHz (mode 2), and 3.8 GHz (mode 3) with acceptable peak gain. These features make it one of its kind that can support several sub-6 GHz 5 G bands with a compact size for wearable applications and sensors.

Data Availability

The data used to support the findings of this study are available from the corresponding author on request.

Conflicts of Interest

The authors declare that they have no conflicts of interest.

Acknowledgments

This work is supported by the Moore4Medical project, funded within ECSEL JU in collaboration with the EU H2020 Framework Programme (H2020/2014–2020) under grant agreement H2020-ECSEL-2019-IA-876190, and Fundação para a Ciência e Tecnologia (ECSEL/0006/2019). This work is also funded by the FCT/MEC through national funds and when applicable cofinanced by the ERDF, under the PT2020 Partnership Agreement under the UID/EEA/50008/2020 project.

References

[1] W. Lin, H. Wong, and R. W. Ziolkowski, "Wideband pattern-reconfigurable antenna with switchable broadside and conical beams," *IEEE Antennas and Wireless Propagation Letters*, vol. 16, pp. 2638–2641, 2017.

[2] S. Ullah, I. Ahmad, Y. Raheem, S. Ullah, T. Ahmad, and U. Habib, "Hexagonal shaped CPW feed based frequency reconfigurable antenna for WLAN and sub-6 GHz 5G applications," in *Proceedings of the 2020 IEEE International Conference on Emerging Trends in Smart Technologies (ICETST)*, pp. 1–4, Karachi, Pakistan, March 2020.

[3] S.-L. Chen, P.-Y. Qin, W. Lin, and Y. J. Guo, "Pattern-reconfigurable antenna with five switchable beams in elevation plane," *IEEE Antennas and Wireless Propagation Letters*, vol. 17, no. 3, pp. 454–457, 2018.

[4] M. A. Towfiq, I. Bahceci, S. Blanch, J. Romeu, L. Jofre, and B. A. Cetiner, "A reconfigurable antenna with beam steering and beamwidth variability for wireless communications," *IEEE Transactions on Antennas and Propagation*, vol. 66, no. 10, pp. 5052–5063, 2018.

[5] I. B. Mabrouk, M. Nedil, T. A. Denidni, and A. R. Sebak, "A novel design of radiation pattern-reconfigurable antenna system for millimeter-wave 5G applications," *IEEE Transactions on Antennas and Propagation*, vol. 68, no. 4, pp. 2585–2592, 2019.

[6] G. Jin, C. Deng, Y. Xu, J. Yang, and S. Liao, "Differential frequency-reconfigurable antenna based on dipoles for sub-6 GHz 5G and WLAN applications," *IEEE Antennas and Wireless Propagation Letters*, vol. 19, no. 3, pp. 472–476, 2020.

[7] Y. Dou, Z. Chen, J. Bai, Q. Cai, and G. Liu, "Two-port CPW-fed dual-band MIMO antenna for IEEE 802.11 a/b/g applications," *Hindawi International Journal of Antennas and Propagation*, vol. 2021, Article ID 5572887, , 2021.

[8] A. Smida, A. Iqbal, A. J. Alazemi, M. I. Waly, R. Ghayoula, and S. Kim, "Wideband wearable antenna for biomedical telemetry applications," *IEEE Access*, vol. 8, pp. 15687–15694, 2020.

[9] X. Liu, Y. Zhang, R. Jiang, Y. Luo, J. Xiang, and Y. Zhou, "A broadband dual-polarized antenna operating in 5G frequency band," in *Proceedings of the 2019 International Symposium on Antennas and Propagation (ISAP)*, pp. 1–3, IEEE, Xi'an, China, October 2019.

[10] K. Saurav, D. Sarkar, and K. V. Srivastava, "A dual-band reconfigurable Yagi–Uda antenna with diverse radiation patterns," *Springer Applied Physics A*, vol. 123, no. 7, pp. 1–8, 2017.

[11] A. Sowmyadevi, P. Mathur, A. R. Chandran, N. Timmons, J. Morrison, and S. Raman, "2.45 GHz pattern reconfigurable antenna for wireless sensor network applications," in *Proceedings of the 2019 URSI Asia-Pacific Radio Science Conference (AP-RASC)*, pp. 1–4, New Delhi, India, March 2019.

[12] A. A. Niyi Dihissou, A. Diallo, P. L. Thuc, and R. Staraj, "Directive and reconfigurable antenna for wireless sensor network to improve link quality between nodes," in *Proceedings of the 2019 IEEE Sensors Applications Symposium (SAS)*, pp. 1–5, Sophia Antipolis, France, March 2019.

[13] M. Abraham and H. Shekhar, "Social spider optimized design configuration of multiband reconfigurable antenna for 5G applications," *Wireless Personal Communications*, vol. 115, no. 2, pp. 1161–1175, 2020.

[14] D. Patron, Y. Liu, and K. R. Dandekar, "A miniaturized reconfigurable CRLH leaky-wave antenna using complementary split-ring resonators," *Hindawi Journal of Electrical and Computer Engineering*, 2018.

[15] U. Habib, A. E. Aighobahi, T. Quinlan, S. D. Walker, and N. J. Gomes, "Demonstration of radio-over-fiber-supported 60 GHz MIMO using separate antenna-pair processing," in *Proceedings of the IEEE International Topical Meeting on Microwave Photonics (MWP)*, pp. 1–4, Beijing, China, October 2017.

[16] L. Ge, Y. Li, J. Wang, and C.-Y.-D. Sim, "A low-profile reconfigurable cavity-backed slot antenna with frequency, polarization, and radiation pattern agility," *IEEE Transactions on Antennas and Propagation*, vol. 65, no. 5, pp. 2182–2189, 2017.

[17] A. Ghaffar, X. J. Li, and W. A. Awan, "A flexible and pattern reconfigurable antenna with small dimensions and simple layout for wireless communication systems operating over 1.65–2.51 GHz," *Electronics*, vol. 10, no. 5, 2021.

[18] S. N. M. Zainarry, N. Nguyen-Trong, and C. Fumeaux, "A frequency- and pattern-reconfigurable two-element array antenna," *IEEE Antennas and Wireless Propagation Letters*, vol. 17, no. 4, pp. 617–620, 2018.

[19] M. Faizal Ismail, A. Kamal, M. Rahim et al., "Dual-band pattern reconfigurable antenna using electromagnetic band-gap structure," *AEU - International Journal of Electronics and Communications*, vol. 130, Article ID 153571, 2021.

[20] R. Dewan, M. K. Abd Rahim, M. R. Hamid, M. Himdi, H. B. A. Majid, and N. A. Samsuri, "HIS-EBG unit cells for pattern and frequency reconfigurable dual band Array antenna," *Progress In Electromagnetics Research M*, vol. 76, pp. 123–132, 2018.

[21] M. K. Shereen, M. I. Khattak, and M. Al-Hasan, "A frequency and radiation pattern combo-reconfigurable novel antenna for 5G applications and beyond," *Electronics*, vol. 9, no. 9, 2020.

[22] B. K. Ahn, H.-W. Jo, J.-S. Yoo, J.-W. Yu, and H. L. Lee, "Pattern reconfigurable high gain spherical dielectric resonator antenna operating on higher order mode," *IEEE Antennas and Wireless Propagation Letters*, vol. 18, no. 1, pp. 128–132, 2019.

[23] Z. Zhu, P. Wang, S. You, and P. Gao, "A flexible frequency and pattern reconfigurable antenna for wireless systems," *Progress In Electromagnetics Research Letters*, vol. 76, pp. 63–70, 2018.

[24] L. Han, C. Wang, W. Zhang, R. Ma, and Q. Zeng, "Design of frequency- and pattern-reconfigurable wideband slot antenna," *International Journal of Antennas and Propagation*, vol. 14, 2018.

[25] I. Ahmad, H. Dildar, W. U. R. Khan et al., "Design and experimental analysis of multiband compound reconfigurable 5G antenna for sub-6GHz wireless applications," *Wireless Communications and Mobile Computing*, vol. 2021, Article ID 5588105, 2021.

[26] M. Robens, R. Wunderlich, and S. Heinen, "UWB LNAs for ground penetrating radar," in *Proceedings of the 2009 IEEE*

International Symposium on Circuits and Systems, pp. 229–232, Taipei, Taiwan, May 2009.

[27] A. Clegg, "C-band & 3.1–3.55 GHz," Google wireless innovation forum," 2021, https://www.wirelessinnovation.org/assets/Webinar_Slides/Spectrum_Sharing_Deep_Dive/Clegg%20-%203.7%20and%203.45%20GHz%20Bands%20for%20WInnForum%20Spectrum%20Sharing%20Workshop.pdf.

[28] T. Khan, M. Rahman, A. Akram, Y. Amin, and H. Tenhunen, "A low-cost CPW-fed multiband frequency reconfigurable antenna for wireless applications," *Electronics*, vol. 8, no. 8, p. 900, 2019.